Journal of
Ceramic Science
and Technology

J. Ceram. Sci. Tech., **03** [01] 41-48 (2012)
DOI: 10.4416/JCST2011-00042
available online at: http://www.ceramic-science.com

Applicability of Common Young's Modulus-Porosity Models to Highly Porous 3D Printed Stoneware Ceramic

G.L.S. Marchelli*, M.A. Ganter, D.W. Storti

University of Washington, Department of Mechanical Engineering, Seattle, WA 98195, USA
received 12 November, 2011; received in revised form 28 November, 2011; accepted 2 December, 2011

Abstract

Purpose: This paper explores the relationship between Young's modulus and porosity in stoneware ceramic parts fabricated by means of three-dimensional printing (3DP) and post-processed via kiln sintering. Porosity, strain, and bulk density vary according to the parameters of the sintering schedule, which in turn affects the mechanical properties of the 3D printed ceramics. It is useful to have a quantitative understanding of this relationship, however, the range of porosity typical to 3DP ceramics lies beyond the intended range of applicability for existing stiffness-porosity models. Here we present experimental measurements of Young's modulus and porosity, and quantitatively evaluate existing models for applicability in 3DP's high porosity range.

Design/Methodology/Approach: Experimental data including strain as a function of peak soak time, e.g. time spent at peak soak temperature, porosity and bulk density as functions of peak soak temperature, and Young's modulus as a function of porosity are presented for 3DP stoneware. A new heating schedule has been adapted to produce lower porosity 3DP stoneware objects to examine the applicability of existing stiffness-porosity relationships. A regression analysis was performed to evaluate the effective range of popular Young's modulus-porosity models.

Findings: Strain was found to be highly dependent on time spent at peak soak temperature and was up to 100 % greater than published values produced by a previous heating schedule. Porosity and bulk density were found to be reasonably modeled as linear functions of peak soak temperature for peak temperatures in the range of 1204 °C to 1316 °C. Use of the current heating schedule allowed for lower than typical porosities in the 3DP stoneware, which led to a broader range of data for fitting the stiffness-porosity models. Optimization of the fitting parameters for the highly porous 3DP stoneware resulted in R^2 values greater than 0.99, indicating the ability to extend popular models to non-conventionally produced ceramics.

Research Limitations/Implications: The 3DP stoneware used exhibited relatively high porosities ranging from 48 % to 64.6 %, and high strain behavior of up to 47 %. Additionally, only strain was explored as a function of peak soak time owing to kiln restrictions; all other variables were measured as functions of peak soak temperature.

Originality/Value: This paper provides the first experimental measurements of the dependence of porosity on relevant sintering parameters for 3DP stoneware ceramics. Analysis of the experimental measurements establishes, for the first time, that application of existing stiffness-porosity models in the higher porosity range requires significant parameter adjustments, with the appropriate parameter values being presented.

Keywords: Printed ceramic, stoneware, stiffness, 3DP

I. Introduction

The framework has been laid for creating new powder and binder systems for use in three-dimensional printers (3DP). Materials such as terra cotta [1], mid- to high-fire ceramics [2], and most recently glass [3–4] have all been adapted for use in powder-based 3DP. More information regarding the formulation of stoneware for use in 3DP can be found in previous works [1–2, 5].

Flynn and Stachurski [6] have thoroughly characterized stoneware produced with conventional manufacturing methods, e.g., throwing, slip casting, and extruding, and this work will be used as a benchmark for representing solid stoneware mechanical properties. Firing curves for 3DP stoneware are not readily available, therefore specifications for a new heating schedule are included later in this section.

The dependence of the elastic properties of ceramics on porosity has been a topic of research for many decades [7–17]. However, most powder-based 3DP technologies produce objects that are inherently porous prior to post-processing (i.e. sintering or infiltration) [5, 18–19]. The significance of the work presented in this paper is to examine a variety of Young's modulus versus porosity models in an effort to quantify and qualify their applicability to 3DP stoneware.

Prior work on 3DP stoneware relied on using a simple flash-fire heating schedule for sintering the 3D printed stoneware specimens [2]. Using the flash-firing heating schedule, it was found that only a limited number of sizes and shapes could be successfully sintered. Many of the

* Corresponding author: grantlsm@uw.edu

objects were susceptible to rupturing, which was due to binder boiling out of the objects, a ramification of excessive ramp rates. In order to produce parts with a wider range of porosities, a more sophisticated heating schedule was developed which includes two low-temperature holds for binder burn-out and a high-temperature soak whose length can be extended to increase shrinkage and reduce porosity. The two low-temperature holds have also allowed for the realization of more complex geometries. This heating schedule, shown in Fig. 1, was adapted from those employed with other 3DP sintered materials [20] and was utilized to produce the new results presented in this paper.

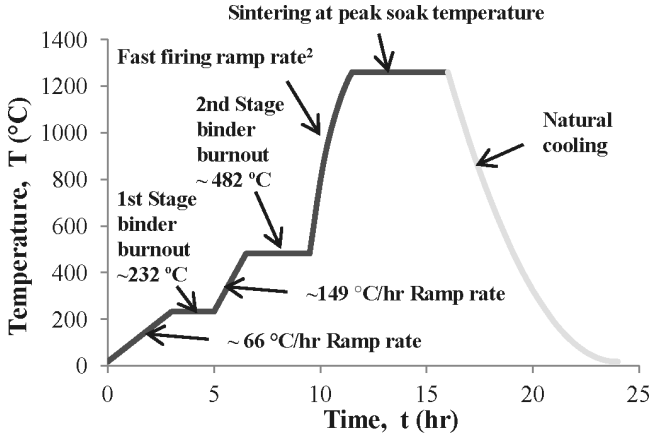

Fig. 1: Three-stage heating schedule developed for experimentation.

The process used to create the 3DP stoneware specimens is a very recent development, so bulk mechanical properties of 3DP stoneware are not available in the literature. This paper presents results of the first engineering tests for strain, bulk density, porosity, and Young's modulus (in compression) for 3DP stoneware using a specially optimized heating schedule. We then compare these results with those found using the flash-firing method from previous efforts and determine appropriate fitting parameters for the Young's modulus-porosity models.

For the duration of this paper, green will refer to specimens that have been 3D printed but not sintered, and brown will refer to specimens that have been both 3D printed and sintered. Green specimens were 3D printed, put through a drying cycle, measured, and then kiln-fired prior to testing. A standard hexagonal pottery kiln, regulated by an Orton AutoFire controller, was utilized to sinter the specimens at maximum temperatures ranging from 1204 °C to 1316 °C, the maximum kiln temperature.

The remainder of this paper is organized as follows. Section II will discuss the various testing methods used during experimentation to determine: 1) the dependence of strain on time at peak soak temperature, 2) porosity as a function of peak soak temperature, 3) bulk density as a function of peak soak temperature, and 4) Young's modulus or stiffness as a function of porosity. Time and temperature play a key role in the sintering of ceramics, with both sintering parameters greatly influencing strain, porosity, and bulk density. As a result, Young's modulus is, in essence, a function of sintering time and temperature. Section III presents our findings for the strain, porosity, bulk density, and Young's modulus experimentation. Section IV provides a discussion of the results, which ultimately ties together the concept of sintering parameter interdependency. Our conclusions are formed in Section V.

II. Methods

(1) Strain Dependence on Sintering Time

Strain, ε, is a dimensionless quantity defined as the change in length per unit length; e.g., $\varepsilon = \Delta L / L_o$. Our previous investigation of strain [2] kept the peak soak time variable constant while varying temperature, but it is widely accepted that the sintering phenomenon depends on several variables including both temperature and time [20–24].

ASTM standard C373–88 on testing whitewares [25] (i.e. porcelain) was chosen because the procedure and test methods outlined in this standard apply to materials most similar to the stoneware that is the focus of this research. Measurements for the width and height were taken at three different points for each specimen using Mitutoyo digital calipers (ABSOLUTE DIGIMATIC), accurate to 0.01 mm, with the average height and width used in the subsequent calculations. A log-log plot of strain as a function of holding time at peak soak temperature (1240 °C) can be found in Fig. 2 a.

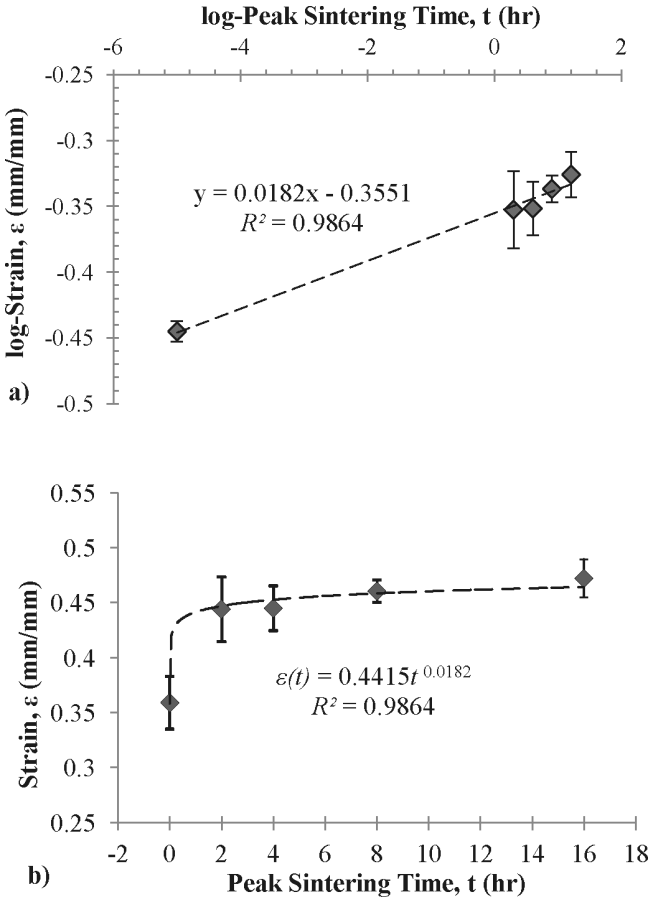

Fig. 2: a) The linear model of log-strain versus log-time at peak soak time with a high coefficient of determination ($R^2 > 0.98$) establishes the exponential relation shown in b). Note the marked increase in strain between a 0-hour hold and a 2-hour hold.

Objects created using 3DP powder systems are frequently subjected to some type of post-processing to increase the relatively low strength of a green part [5]. Post-processing has a number of benefits including increased green strength, improved surface finish, and the ability to impart a smoother texture in a printed part. Materials that cannot be fired, such as some plasters and wood-based powders, can be infiltrated or impregnated with waxes or epoxies [5]. Since the specimens have a predominantly open-cell, interconnected network of pores, capillary action drives infiltration to produce a near fully dense object. 3DP systems that use metals and ceramics as a printing medium produce parts that can be sintered to increase strength and density. A phenomenon known as densification occurs within the specimen during sintering, which is the result of a variety of processes including neck growth, grain growth, and pore shrinkage [20–24]. German [23] has shown that during the adhesion/initial stages of sintering, partial necking is apparent between the powder particles, indicating that densification has begun [20–24]. Pores elongate during the intermediate stage of sintering, which greatly affects the densification rate, and therefore the density of the specimen [23]. As a result of the densification or closing of pores, the parts undergo strain; Figs. 2 and 4 demonstrate this phenomenon, with both strain and density rising with increasing degrees of sintering.

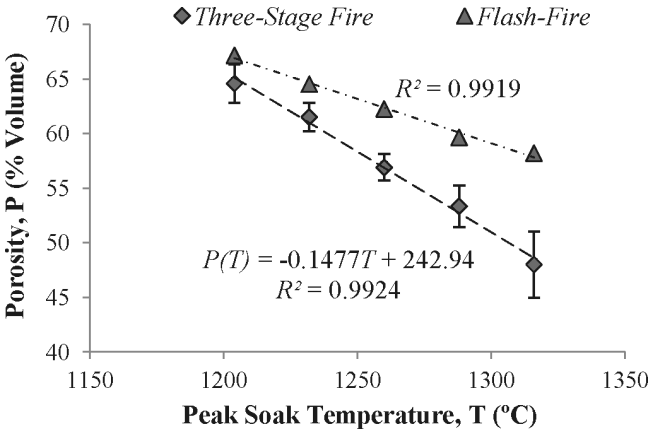

Fig. 3: Porosity as a function of the peak soak temperature. Note the trend; as the peak soak temperature increases, the difference between the porosities also increases. This trend can be attributed to longer exposure to elevated temperatures, which in turn increases densification within the specimen.

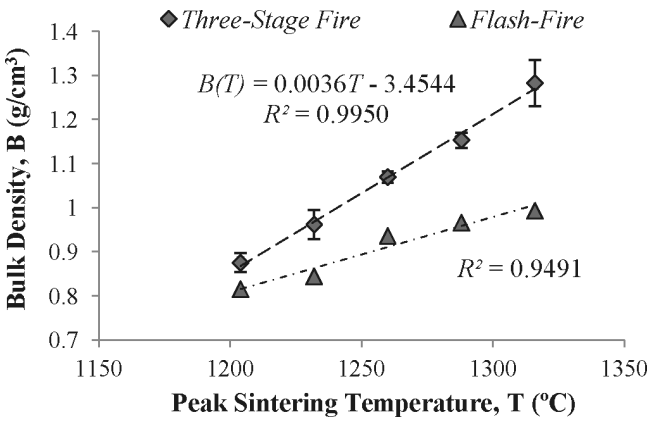

Fig. 4: Bulk density as a function of peak soak temperature using the three-stage firing compared to the flash-firing heating schedules.

Specimens were sintered using the heating schedule in Fig. 1 and porosity was measured according to ASTM standard C 373 – 88. With an Archimedes-type testing apparatus, the specimens were weighed using an OHAUS® Adventurer™ scale, accurate to 0.001 g. The density of the water ϱ_w used in subsequent porosity and density computations was recorded at 0.9982 g/cm^3 at a temperature of 20.2 °C. Calculations for the apparent porosity P and the bulk density B were performed using the equations found in [25].

(2) Young's Modulus as a Function of Porosity

Many different theoretical and empirical models have been proposed relating Young's modulus to porosity for brittle ceramic materials [7–17]. As described above, our specimens were produced using a powder-based type of 3D printing process which is susceptible to a high volume fraction of porosity, due to organic burn-out and low packing density. However, porosity is not always considered a negative property; porous ceramics are used as refractory [11] materials and as scaffolds in tissue engineering applications [26]. The mechanical properties of a porous ceramic are largely dependent on pore distribution, shape, and size, but most investigators assume evenly distributed, uniformly sized, spherical pores for simplicity [8, 11, 14–15, 27]. While these investigators pursue the idealized porosity model, more recent developments geared towards the representation of heterogeneous solids, in the context of tissue engineering, have been made by Sun *et al.* [28]. These models may provide new insights aimed at modeling the mechanical properties of ceramics with stochastic porosity. However, for simplicity, the porosity model used this paper is limited to the idealized case.

We processed the 3D printed specimens by firing them at temperatures in the 1204 – 1316 °C range. Following sintering, we subjected the specimens to uniaxial compressive loading using an Instron Universal Testing Machine (model # 5585H), in accordance with ASTM standard C 373 – 88 [25]. Experimental conditions were as follows: a cross-head speed of 1 mm/min using a 100 kN load-cell, with typical room temperature (~22 °C) and relative humidity. Following data acquisition, models presented in the subsequent section were used for regression analysis and parameter optimization.

(3) Review of Young's Modulus-Porosity Models

Over the last few decades, there has been much exploration into the mechanical characterization of brittle porous ceramics and their dependence on porosity, as revealed by Boccaccini and Fan [17]. The models used in this study were chosen to cover the range of functional dependences (polynomial-, power-, and exponential-type) commonly used and cited in the literature.

After thorough examination of previous work done in the area of porous ceramics, Spriggs [12] proposed an expression of the form:

$$E = E_0 \cdot e^{-bP} \quad (1)$$

where E is Young's modulus, E_0 is the zero-porosity Young's modulus, P is the porosity, and b is an empiri-

cal constant. Wang [7] has proposed a slightly more general expression in the form of an exponential quadratic:

$$E = E_0 \cdot e^{-(bP+cP)^2} \quad (2)$$

where, b and c are materials constants [7–8]. While investigating porous alumina, Phani and Niyogi [8], aiming to account for variations in pore connectivity, derived a semi-empirical power model:

$$E = E_0 \cdot (1 - aP)^n \quad (3)$$

where, a and n are material constants. Work by Wagh, Poeppel, and Singh [14] revealed that the material constant a in Eq. (3) is related to the packing density and critical porosity of the material and fitting of experimental data consistently results in the material constant, a, being equal to unity [8, 14]. As a result, Wagh, Poeppel, and Singh [14] suggested the following relation that assumes a random pore size and distribution:

$$E = E_0 \cdot (1 - P)^m \quad (4)$$

where, m is a material constant. MacKenzie [27] presented a semi-empirical, quadratic formula that has been used to fit a wide variety of experimental data for the elastic modulus of porous ceramics [14–15]:

$$E = E_0 \cdot (1 - f_1 \cdot p + f_2 \cdot p^2) \quad (5)$$

where, E and E_0 are the Young's modulus and the zero-porosity Young's modulus, respectively, p is the volume fraction of porosity, and f_1 and f_2 are fitting parameters [14, 27].

III. Results

Experimental results for strain, bulk density, porosity, and stiffness-porosity fitting are presented below in the form of tables and figures. We discovered that soak time at peak temperature had a profound effect on strain. Porosity as a function of peak soak temperature decreased at a higher rate and was lower overall when compared to the flash-fire approach. Bulk density increased and was higher overall when compared to the flash-fire approach. The fitting parameters for each stiffness-porosity model were successfully optimized and generated good fits ($R^2 > 0.99$) for high-porosity 3DP stoneware ceramics.

IV. Discussion

(1) Strain as a Function of Time

Using a least squares fit approach to the *log*-strain versus *log*-time data, a linear dependence was found of the form $log(\varepsilon(t)) = mlog(t) + log(a)$ where, $\varepsilon(t)$ is strain as a function of holding time at peak soak temperature t, m is the slope, and a is the intercept. A high R^2 was found, 0.9864, indicating that the log-linear model was in good agreement with the experimental data. A good fit of the log-linear model to the experimental data also reveals that a power-type relationship exists between the strain and the holding time of the form $\varepsilon(t) = \beta t^m$, where m is the slope of the linear fit to the *log-log* plot, and β is the *strain coefficient* defined by $\beta = 10^a$. These results differ greatly from the strain versus peak soak temperature found in [2], which exhibited purely linear behavior. In this experimentation, strain was measured by maintaining the peak soak temperature at 1260 °C and varying the holding time from 0 to 16 hours. The strain found using this method ranged from 0.3589 mm/mm at a 0-hour hold, to 0.4722 mm/mm at a 16-hour hold. By comparing the 0-hour hold time results given in [2] and in this manuscript, a 106 % difference is realized, indicating that time spent at peak temperature has a profound effect on the sintering phenomenon (see Fig. 2 b). The increased strain found by varying peak soak time also yielded a reduction in porosity for the 3DP stoneware. As the pores shrink during densification, the specimen is subjected to increased strain, with the final outcome being a smaller, but less porous specimen. The reduction in porosity is in turn related to the increase in stiffness, as apparent in Figs. 5 – 7.

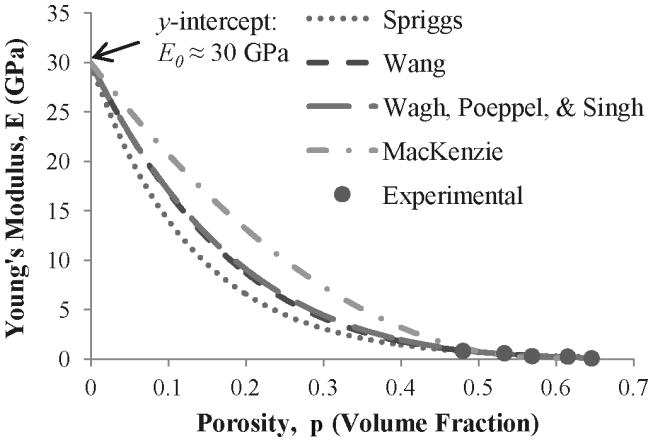

Fig. 5: Experimental data plotted with the Young's modulus-porosity models. Note the value of the y-intercept, which is consistent with the average zero-porosity Young's Modulus: 30 GPa in [6].

(2) Apparent Porosity and Bulk Density

A least squares method was employed to fit both the porosity and bulk density data, which resulted in a high R^2 for both cases ($R^2 > 0.99$). Linear models were found to be $P(T) = -0.148T + 242.9$ and $B(T) = 0.004T - 3.454$ for the porosity and bulk density, respectively, where porosity P and bulk density B are functions of the peak soak temperature T. A comparison of the porosity and bulk density using the fast-firing method reiterates that time has a significant effect (see Figs. 3 and 4) on the sintering phenomenon in 3DP objects. Specimens produced in a 3DP powder system that are then sintered *typically* can only achieve relative densities of 40 – 60 % by volume without applying mechanical compaction or a pressurized atmosphere [29–30]. The material system used in this testing comprised approximately 33 % organics by volume [1–2]. During sintering, the organics, which make up 33 % of the 3DP stoneware by volume, burn out of the specimen and therefore the specimen loses approximately 33 % of its green volume. Because 3DP specimens frequently achieve a relative density of 40 – 60 %, a 33-% loss of volume due to organic burn-out results in specimens with relative densities of approximately 20 – 40 % and apparent porosities of 60 – 80 %. Using the newly adapted multi-stage heating schedule, apparent porosities ranging from 48.0 % to 64.6 % were found, which are 3.98 – 21.3 % lower than the apparent porosities revealed in previous works. The

resulting porosity range is also lower than the 60 – 80 % predicted range.

Our results indicate that longer sintering times allow for greater development of intermediate stage sintering and therefore further densification within the specimen [20 – 24]. Bulk densities ranging from 0.876 – 1.28 g/cm^3 were attained, which are 6.91 – 22.6 % higher than the bulk densities presented in previous work. It is worth noting that as the peak soak temperature increases, the difference between the flash-fired data and the data presented in this manuscript, for both porosity and bulk density, also increases. As the porosity decreases and the bulk density increases, the specimens experience an increase in mechanical stiffness. The exponential rise in Young's modulus (Fig. 7) is the result of increased necking, or densification, and a corresponding diminution of porosity. Densification and reduced porosity are directly correlated to increased exposure at elevated sintering temperatures.

(3) Young's Modulus-Porosity Regression Analysis

Many of the investigators of Young's modulus-porosity models have suggested limitations that include pore shape and particle size distribution to the fitting equations [7 – 12, 16, 31]. A typical restriction lies within the range of porosities that can be used by the models, with most being applicable to porosities $p \leq 0.5$ [7 – 8, 17]. 3DP stoneware ceramics resulted in high porosities $p \geq 0.48$; therefore, we were interested in models that fit the data at the high-end of the functional porosity spectrum. To test the validity of the models, we minimized the error between the experimental data and the fitting equations by optimizing the fitting parameters. Flynn and Stachurski [6] calculated the zero-porosity Young's modulus, E_0, of stoneware clay bodies and reported 30 (±15) GPa. Using the models given above, we were able to fit the data in the high-porosity range with high accuracy, while simultaneously attaining a zero-porosity Young's modulus that was in agreement with the accepted published value of 30 GPa [6]. A table revisiting the different models incorporated in fitting the experimental data, as well as their respective fitting parameters, zero-porosity Young's modulus, and R^2 values, is shown below.

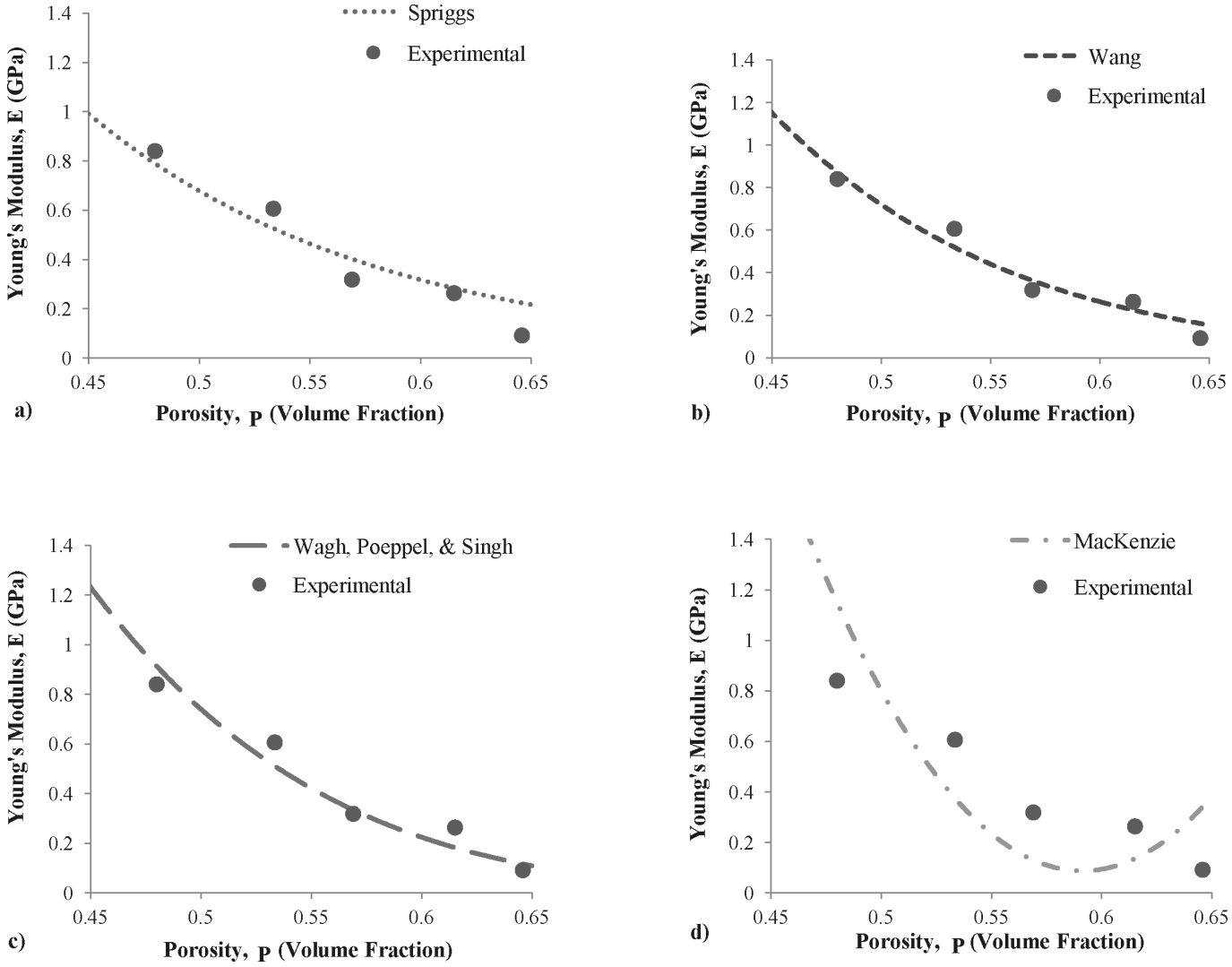

Fig. 6: An isolated view of the experimental data and a) Sprigg's [11], b) Wang's [6], c) Wagh, Poeppel, and Singh's [13], and d) MacKenzie's [27] models, respectively.

Table 1: Test parameters and results obtained from fitting experimental data with the following Young's modulus-porosity relationships.

Model:	$E = E_0 \exp[-bP]$	$E = E_0 \exp[-(bP + cP^2)]$	$E = E_0(1 - P)^m$	$E = E_0(1 - f_1P + f_2P^2)$
Source:	Spriggs	Wang	Wagh, Poeppel, & Singh	MacKenzie
	E_0 = 30.0 GPa	E_0 = 29.9 GPa	E_0 = 29.9 GPa	E_0 = 29.9 GPa
	b = 7.57	b = 5.30	m = 5.34	$f1$ = 3.37
	$\boldsymbol{R^2}$ = 0.9999	c = 4.31	$\boldsymbol{R^2}$ = 0.9999	$f2$ = 2.85
		$\boldsymbol{R^2}$ = 0.9999		$\boldsymbol{R^2}$ = 0.9996
		Average E_0 = 29.9 ± 0.005 GPa		

We have measured porosity and stiffness for 3DP stoneware ceramics and provide necessary adjustments to parameter values in Table 1. Prior to alteration of the fitting parameters found in the literature, the various models yielded R^2 values of less than 0.8, however, by optimizing the parameters to fit the data and the average zero-porosity Young's modulus given by Flynn and Stachurski[6], we were able to generate R^2 values greater than 0.99 for all models in the high porosity range. Despite Eq. (1) being derived empirically by Spriggs [12] for a unique set of conditions [8], the model was still found to accurately fit the data. Wang [7] theoretically derived Eq. (2) allowing for a broader porosity range and varying powder size; these characteristics made it ideal for modeling newly developed material systems [7–8]. It is worth noting that the quadratic model given by MacKenzie [27] reaches a minimum at $p \approx 0.59$, indicating that stiffness should be increasing for porosities greater than $p = 0.59$ (see Fig. 6 d), an unphysical phenomenon for this particular ceramic material formed using 3DP. This resulted in a slightly less accurate fit, because the highest porosity found during experimentation for the 3DP stoneware was approximately $p = 0.65$.

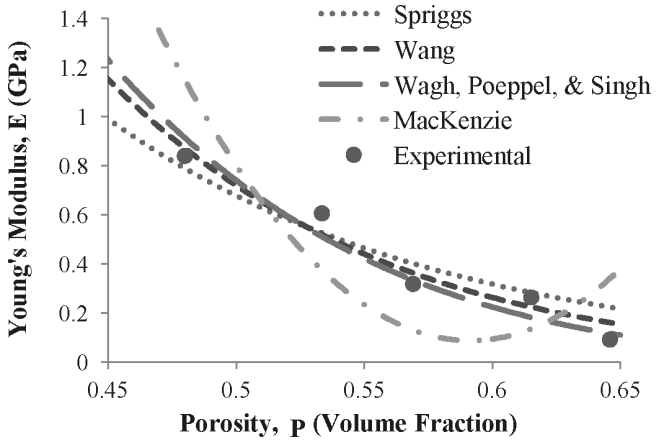

Fig. 7: A closer look at the experimental data plotted with the Young's modulus-porosity models. Note that all models are in good agreement with the data.

V. Conclusions

Experimental data for strain as a function of time held at peak soak temperature, porosity and bulk density as functions of peak soak temperature, and Young's modulus as a function of porosity were presented. An adapted three-stage heating schedule has been presented that contains multiple ramp rates and isothermal soaks (to accommodate for organic binders burning out and achieve relatively high strain), which has been implemented in the post-processing of the 3DP stoneware used in this study. We quantified the effects of flash-firing versus three-stage firing. Our new heating schedule enables the fabrication of lower porosity 3DP stoneware. By producing lower porosity specimens, we were able to work slightly beyond the upper porosity limits of most Young's modulus-porosity models. We examined these relationships to determine whether or not the application range could be extended into highly porous 3DP stoneware and found the former to be true.

Strain as a function of holding time at peak soak temperatures in the range of 1204 °C to 1316 °C for 3DP stoneware behaves logarithmically and was found to be up to 100 % larger than the strain found in the literature for flash-firing. The porosity of the specimens was found to decrease by up to 21.3 %, while the bulk density increased by up to 22.6 % when the three-stage heating schedule was applied over the range of temperatures studied. Both the porosity and the bulk density are reasonably modeled as linear functions of peak soak temperature for fixed sintering time. Strain was found to behave as a linear function of peak soak temperature and compressive strength followed an exponential function dependent on specimen density. Advanced densification allows for increased mechanical strength via an increase in particle bonding and a resulting decrease in pore size. The stiffness of 3DP stoneware was greatly influenced by peak soak temperature. This study revealed that stiffness of 3DP stoneware varies greatly with peak soak temperature. The use of fitting parameters given in the literature for the stiffness-porosity relations resulted in poor fits to the data ($R^2 < 0.8$). By optimizing the parameters, we were able to achieve very accurate fits to 3DP experimental data; R^2 values exceeding 0.99 were found for all models investigated. However, the quadratic developed by MacKenzie [27] is not recommended for use in highly porous ceramics; using our parameters, the elastic modulus of the stoneware predicted by the model began

to increase after reaching a global minimum at a porosity of approximately 59 %. Our results indicate that the functional form of the remaining models used to relate porosity and Young's modulus for low-porosity, traditionally manufactured ceramics can be applied to highly porous 3DP stoneware with appropriate adjustments to parameter values as specified in Table 1.

Acknowledgements

We would like to thank our staff engineer, Bill Kuykendall, for his assistance with setting up the compression test using the INSTRON Universal Testing Machine (model 5585H).

References

1 Ganter, M., Storti, D., Utela, B.: The printed pot, in: Ceramics Monthly. Ceramic Publications Company, Westerville, Ohio, **36**, (2009).

2 Marchelli, G., Ganter, M., Storti, D.: New material systems for 3D ceramic printing, in: Proceedings of the Twentieth International Solid Freeform Fabrication Symposium. University of Texas, Austin, TX, (2009).

3 Marchelli, G., Prabhakar, R., Ganter, M., and Storti, D.: An introduction to 3D glass printing, in: Proceedings of the Twentieth International Solid Freeform Fabrication Symposium. University of Texas, Austin, TX, (2010).

4 Marchelli, G., Storti, D., Prabhakar, R., Ganter, M.: The guide to 3D glass printing: Developments, methods, diagnostics and results. *Rapid Prototyping J.*, **17,** (3), (2011).

5 Utela, B., Storti, D., Anderson, R., and Ganter, M.: A review of process development steps for new material systems in three-dimensional printing (3DP). *J.Manuf. Process.*,**10,** (2), 96 – 104, (2008).

6 Flynn, A.J., Stachurski, Z.H.: Microstructure and properties of stoneware clay bodies. *J. Fine Part, Sci.: Clay Miner.*, **41,** (3), 775 – 789, (2006).

7 Wang, J.C.: Young's modulus of porous materials, *J.Mater. Sci.*, **19,** (3), 801 – 808, (1984).

8 Phani, K.K., Niyogi, S.K.: Young's modulus of porous brittle solids, *J.Mater. Sci.*, **22,** (1), 257 – 263, (1987).

9 Nielsen, L.F.: Strength and stiffness of porous materials, *J. Am. Ceram. Soc.*, **73**, (9), 2684 – 2689, (1990).

10 Ramakrishnan, N., Arunachalam, V.S.: Effective elastic moduli of porous ceramic materials, *J. Am. Ceram. Soc.*, **76,** (11), 2745 – 2752, (1993).

11 Kováčik, J.: Correlation between Young's modulus and porosity in porous materials, *J. Mater. Sci. Lett.*, **18**, (13), 1007 – 1010, (1999).

12 Spriggs, R.M.: Expression for effect of porosity on elastic modulus of polycrystalline refractory materials, particularly aluminum oxide, *J. Am. Ceram. Soc.*, **44**, (12), 628 – 629, (1961).

13 Dean, E.A., Lopez, J.A.: Empirical dependence of elastic moduli on porosity for ceramic materials, *J. Am. Ceram. Soc.*, **66,** (5), 366 – 370, (1983).

14 Wagh, A.S., Poeppel, R.B., Singh, J.P.: Open pore description of mechanical properties of ceramics, *J. Mater. Sci.*, **26,** (14), 3862 – 3868, (1991).

15 Wagh, A.S., Singh, J.P., Poeppel, R.B.: Dependence of ceramic fracture properties on porosity, *J. Mater. Sci.*, **28,**(13), 3589 – 3593, (1993).

16 Coble, R.L., Kingery, W.D.: Effect of porosity on physical properties of sintered alumina, *J. Am. Ceram. Soc.*, **39**, (11), 377 – 385, (1956).

17 Boccaccini, A.R., Fan, Z.: A new approach for the Young's modulus-porosity correlation of ceramic materials, *Ceram. Int.*, **23,** (3), 239 – 245, (1997).

18 Sachs, E.M., Cima, M., Cornie, J.: Three-dimensional Printing: Rapid tooling and prototypes directly from a CAD model, *CIRP Ann.-Manuf. Techn.*, **39**, (1), 201 – 204, (1990).

19 Sachs, E.M., Haggerty, J.S., Cima, M.J., *et al.*: Three-dimensional printing techniques, in U.S. Patent and Trademark Office, MIT, Editor, United States, (1993).

20 Johnston, S.R.: Initial Stage Sintering Model of 316L Stainless steel with application to three dimensionally printed (3DP™) components, in Mechanical Engineering, University of Washington, Seattle, 10 – 11, 25 – 30, (2005).

21 Kuczynski, G.C., Sintering processes, in materials science research., Plenum Press: New York, (1980).

22 Bourell, D.L., Marcus, H.L., Barlow, J.W., Beaman, J.J.: Selective laser sintering of metals and ceramics, *Int. J. Powder Metall.*, **10,** (4), 369 – 381, (1992).

23 German, R.M.: Sintering theory and practice, New York: John Wiley & Sons, Inc., (1996).

24 Rahaman, M.N.: Sintering of ceramics, Boca Raton: CRC Press, (2008).

25 ASTM. Standard test method for water absorption, bulk density, apparent porosity, and apparent specific gravity of fired whiteware products, West Conshohocken, (2006).

26 Seitz, H., Rieder, W., Irsen, S., Leukers, B., Tille, C.: Three-dimensional printing of porous ceramic scaffolds for bone tissue engineering, *J. Biomed. Mater. Res, B Appl. Biomater.*, **74,** (2), 782 – 8, (2005).

27 MacKenzie, J.K.: The elastic constants of a solid-containing spherical holes. *P. Phys. Soc. Section B*, **63,** (1), (1950).

28 Schroeder, C., Regli, W.C., Shokoufandeh, A., Sun, W.: Representation of porous artifacts for bio-medical applications, in: Proceedings of the Eighth ACM Symposium on Solid Modeling and Applications. ACM, Seattle, WA, (2003).

29 Sachs, E.M., Cima, M., Caradonna, M.A., Grau, J., Serdy, J.G., Saxton, P.C., Uhland, S.A., Moon, J.: Jetting layers of powder and the formation of fine powder beds thereby, U.S.P.a.T. Office, Editor. Massachusetts Institute of Technology, (2003).

30 Baskaran, S., Graff, G.L.: Method of freeform fabrication by selective gelation of powder suspensions, U.S.P.a.T. Office, Editor. Battelle Memorial Institute, (1997).

31 Ramakrishnan, N. *et al.*: Effective elastic moduli of porous solids, *J.Mater. Sci.*, **25,** (9), 3930, (1990).